

Friction Stir Processed AA5182-O and AA6111-T4 Aluminum Alloys. Part 1: Electron Backscattered Diffraction Analysis

Sumit Agarwal, Clyde L. Briant, Louis G. Hector Jr., and Yen-Lung Chen

(Submitted January 9, 2007; in revised form March 9, 2007)

The present article is the first part in a two-part series in which crystallographic texture developed during friction stir processing of AA5182-O and AA6111-T4 is characterized and its impact on tensile properties explored. For the texture measurements, coupons were cut from the friction stir processed zone at selected orientations relative to the direction of tool translation. Texture was characterized with electron backscatter diffraction (EBSD) in a scanning electron microscope. Measurements were made at key positions along the coupon surfaces and texture differences between the two friction stir processed Al alloys are discussed in detail. Grain size variations were also measured in both the base and friction stir processed materials and subsequently compared. In part 2, a state-of-art digital image correlation technique is used to investigate tensile properties of both friction stir processed Al alloys. The impact of crystallographic texture on mechanical properties is also explored in this latter part.

Keywords aluminum alloys AA5182-O AA6111-T4, electron backscattered diffraction, friction stir processing

1. Introduction

The reduced weight and high strength-to-weight ratio of Al alloys makes them desirable alternatives to ferrous materials in specific automotive applications. However, some significant challenges remain in the large-scale implementation of Al alloys in the automotive industry. One of these pertains to the selection of joining methodologies and how these methodologies impact the mechanical integrity of Al structures. Another and perhaps more daunting issue is the joining of dissimilar materials such as Al and steel, and Al and Mg.

Friction stir welding is a relatively new solid-state joining process in which a rotating tool is plunged into and then translated across the joint line between two metal sheets (Ref 1). Friction between the rotating tool (which consists of a threaded pin surrounded by a shoulder region) and the surface, produces temperatures which are in upwards of 80% of the melting point of the metal. A plastically worked zone is generated around the tool due to subsequent material softening leading to transference of joined material from the leading to the trailing edge of the tool. Characteristic “bands” appear

in the wake of the tool after each complete rotation; these bands are evident on the surface of the weld track. The resulting complex flow patterns have been the subject of ongoing research (Ref 2, 3) since these are related to joint properties. Schneider and Nunes (Ref 3) identified three key zones in a friction stir processed material. The first zone inwards from the base material is the heat affected zone (HAZ), wherein significant hardness gradients are found. The next zone is the thermomechanical zone (TMAZ) in which thermomechanical deformation is prevalent. The third zone is the stir zone (SZ) which contains dynamically recrystallized grains and has a characteristic weld nugget geometry that is similar to the joints produced with more conventional processes.

Friction stir welding is advantageous in that it does not involve any melting, does not require filler materials, and does not produce fumes, weld spatter, or arc glare (Ref 4). Although commonly applied to join Al, friction stir welding has been used to join copper, lead, and Mg alloys which are otherwise difficult to join with conventional fusion welding techniques. In fact, friction stir welded Al materials display several advantages over fusion welded Al alloys. These advantages include improved weld strength, and the elimination of porosity and solidification cracking (Ref 5). Mazda announced in late 2005 that friction stir welding had been successfully applied to join an Al alloy to galvanized sheet steel in a component of the 2006 MX-5 sports car (Ref 6).

Crystallographic texture often contributes to anisotropic mechanical properties. An important technique for texture characterization in metals is electron backscattered diffraction (EBSD) (the EBSD technique is described in detail in Schwartz et al. (Ref 7). While the EBSD technique has been widely used to investigate texture in Al alloys, it has only recently been used to investigate texture in Al welds. Most of the texture studies relative to Al weld materials have focused on friction stir welds (Ref 3, 5, 8) and these studies have reported heterogeneous

This article was presented at Materials Science & Technology 2006, Innovations in Metal Forming symposium held in Cincinnati, OH, October 15-19, 2006.

Sumit Agarwal, Applied Materials, Inc, 21515 N.W. Evergreen Parkway, Hillsboro, OR 97124; Clyde L. Briant, Brown University, Providence, RI 02912; Louis G. Hector Jr., and Yen-Lung Chen, General Motors Research and Development Center, 30500 Mound Road, Warren, MI 48090. Contact e-mail: louis.hector@gm.com.

texture variations. For example, Sato et al. (Ref 9) found that the weld center in AA6063 contains a recrystallized grain structure with a shear texture component containing both $\{110\}$ $\langle 001 \rangle$ and $\{114\}$ $\langle 221 \rangle$ orientations. In their studies of texture in friction stir welded AA1100 and AA6061, Field et al. (Ref 5) concluded that severe gradients in crystallographic texture are found in the welds and generally one or more ideal fcc shear textures predominates. Using EBSD, Jin et al. (Ref 10) found a dynamically recrystallized fine grain structure in the weld zones of AA5754 and AA5182 joints. At present, the extent to which crystallographic texture impacts tensile properties of friction stir processed Al alloys is largely unknown.

In the present article, we investigate the texture of friction stir processed AA5182-O and AA6111-T4 alloys, which are common automotive materials, using EBSD. Variations in texture, as suggested by other reports (Ref 3, 5), are characterized in detail from coupons cut from single stir processed tracks on sheets of both materials (no joint materials are considered). In addition, variations in grain size and microstructure are also analyzed and compared with the corresponding base material alloys. This is the first part in a two-part series on crystallographic texture and mechanical property characterization of friction stir processed Al alloys. In Part 2, a state-of-art digital image correlation technique is used to investigate tensile properties of both friction stir processed Al alloys. Since there is a dearth of information linking texture and mechanical properties of friction stir processing materials, the impact of crystallographic texture on tensile properties is also explored in this latter part in order to tie up results from both parts.

The remainder of this article is organized as follows. In Section 2, we summarize salient experimental details. In Section 3, results from EBSD analysis of specific regions within the friction stir processed zones of each alloy are presented. Additional discussion of the results is provided in Section 4, and concluding remarks are presented in Section 5.

2. Experimental

2.1 Friction Stir Processing Parameters

A schematic of the friction stir processing technique is shown in Fig. 1. The friction stir tool is plunged into the sheet material with the profiled pin penetrating to a depth of greater

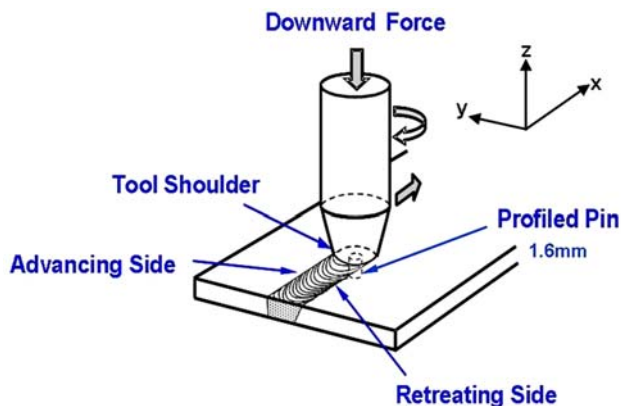


Fig. 1 Schematic of the friction stir processing technique

than 50% of the sheet thickness. Frictional heating plasticizes material beneath the tool and the profiled pin, which is threaded, “stirs” this plasticized material from the front to the back of the sheet/tool conjunction. Rotational and translational speeds were held constant at 1800 rpm and 8 mm/s, respectively, giving a pitch of 268 μm . The pitch is the centerline distance between overlapping bands shed in the wake of the tool following one complete rotation. Loads were maintained at 3.23 kN for AA5182-O and 3.5 kN for AA6111-T4. The tool was H-13 tool steel with a shoulder diameter of 10 mm and was translated along the rolling direction of each sheet. The threaded pin was 1.6 mm in length. Single friction stir processed tracks with a 10 mm width were generated in each sheet.

2.2 Aluminum Alloys

The sheet materials examined in this work were AA5182-O (2.0 mm thickness) and AA6111-T4 (2.6 mm thickness). The AA5182-O alloy is a solid solution strengthened material that is commonly used for automotive structural components. AA6111-T4 is a solution treated and naturally aged alloy that is often employed for automotive body panels due to its relatively high strength and good dent resistance. Typical chemical compositions and thermophysical properties of these alloys are listed in Table 1 and 2 and published tensile properties at ambient temperature are listed in Table 3 (Ref 11).

The microstructure of the material in the advancing side (where the translational and rotational motions of the tool are in the same direction) is typically found to be different from that in the retreating side where the translational and rotational motions of the tool are in opposite directions. Figure 2(a) is a cross-section of a AA5182-O friction stir processed zone. The

Table 1 Typical chemical compositions (wt.%) of alloys used in this study (Ref 11)

Alloy	Fe	Si	Cu	Mn	Mg
6111	0.40 max	0.6-1.1	0.5-0.9	0.1-0.45	0.50-1.0
5182	0.35 max	0.20 max	0.15 max	0.20-0.50	4.0-5.0

Table 2 Thermophysical properties of aluminum. Data taken from (Ref 11)

Alloy	AA5182-O	AA6111-T4
Liquidus temperature, $^{\circ}\text{C}$	638	652
Coherency temperature, $^{\circ}\text{C}$	617	629
Solidus temperature, $^{\circ}\text{C}$	577	582
Thermal conductivity, W/mm K	0.126	0.167
Volumetric heat capacity, $\text{Ws/mm}^3 \text{K}$	0.0027	0.0027

Table 3 Available mechanical properties of materials used in this study. Data taken from (Ref 11)

Alloy	Yield strength, MPa	Ultimate strength, MPa	Elongation, %
6111-T4165	285		25
5182-O 130	275		21

layering on the left side of the stir processed zone is associated with the advancing side as shown in Fig. 1 (the tool motion is outward from the image in Fig. 2a). This layering is less obvious in Fig. 2(b) which is a cross-section of a AA6111-T4 friction stir processed zone.

2.3 Coupon Geometry

Coupons were fabricated from the friction stir processed tracks in each sheet using electrical-discharge machining (EDM). Figure 3(a) shows the as-machined coupon geometry which was chosen to facilitate both the EBSD measurements in the present work and tensile properties measurement via digital image correlation (Part 2 (Ref 12)). The coupons were 50 mm in overall length with a 10 mm gripper width. Two arcs, with a 51.2 mm radius, formed the opposite sides of a 20 mm-long gage section, as shown. The curved gage section geometry ensured that localization and failure occurred at the gage section center in the tensile tests, which had a minimum width of 5 mm. The gage section of each coupon machined from the friction stir processed tracks consisted almost entirely of friction stir processed material.

All EBSD measurements were made from selected tensile coupons from both alloys. Some tensile coupons were sliced parallel to the friction stir processing direction in the xy plane (i.e., longitudinal sections as shown in Fig. 3(b) with the associated coordinate system following that in Fig. 1) so that we could examine up to six internal material surfaces; the corresponding numbering scheme for these internal surfaces is

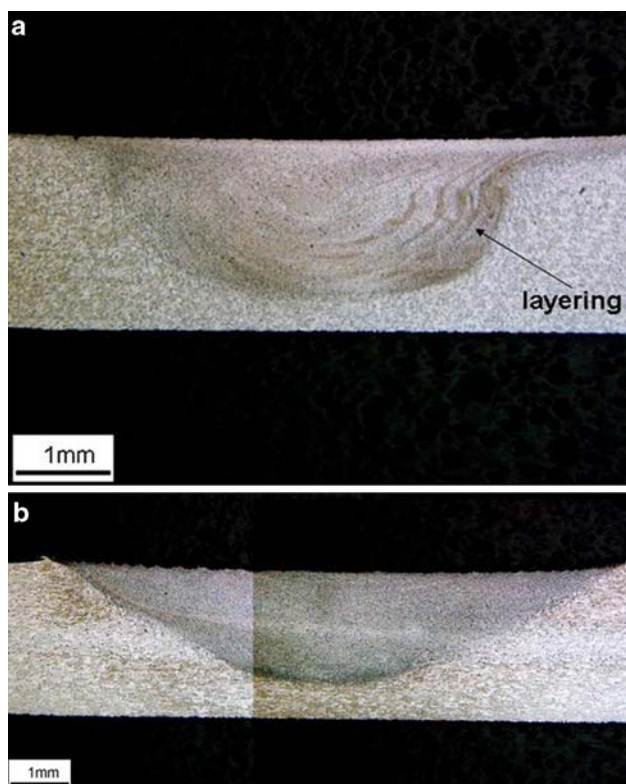


Fig. 2 Optical micrographs showing cross-sections of friction stir processed zones for AA5182-O (a) and AA6111-T4 (b) alloys. (a) Optical micrograph showing cross-section of friction stir processed AA5182-O. (b) Optical micrograph showing cross-section of friction stir processed AA6111-T4

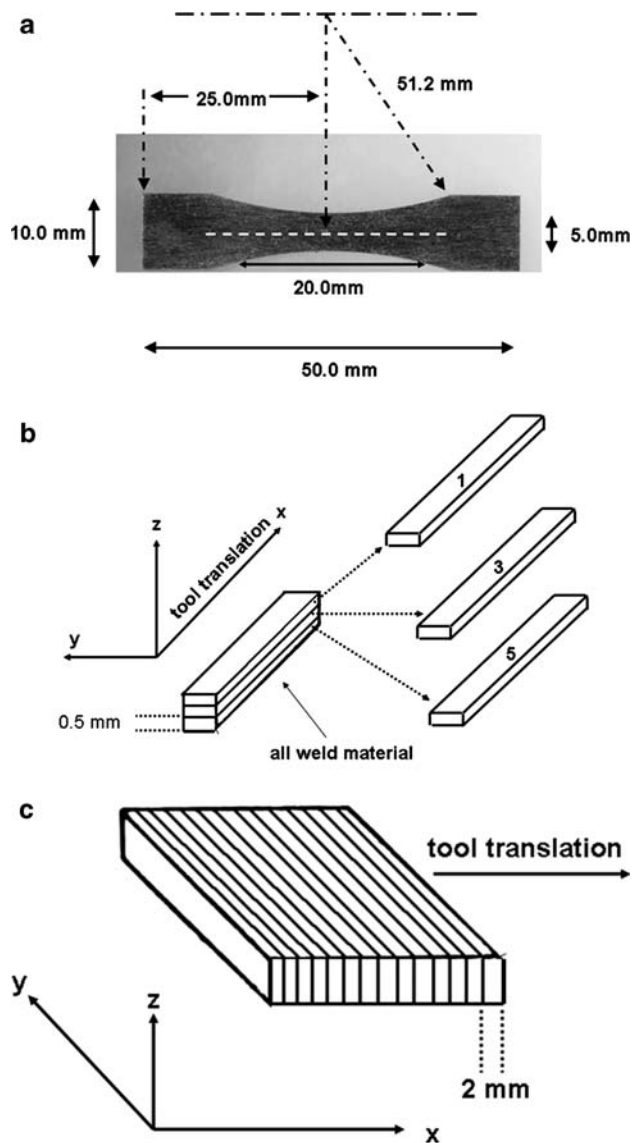


Fig. 3 Coupon geometries. (a) Aluminum tensile coupons consisting almost entirely of friction stir processed material were machined into the above geometry using electrical-discharge machining. (b) Longitudinal sections, consisting entirely of friction stir processed material in its gage section, were cut in the transverse (xy) plane (see Fig. 1) through the coupon thickness. Tool translation is along x . Tool contact is with surface 1. Even numbered surfaces are on the flip side of those shown. (c) Transverse sections, which allowed for examination of texture differences across the stir processed zone, were cut in the transverse (yz) plane (see Fig. 1). Tool translation is along x

given in Table 4. We refer to these coupons as longitudinal sections. In addition, rectangular coupons were cut along the thickness direction (transverse or perpendicular to the tool translation direction, in the yz plane in Fig. 3(c), with the associated coordinate system following that in Fig. 1) such that texture variation across the friction stir zone and into the base material could be readily examined. We refer to these as transverse sections.

For examination with EBSD, each coupon surface was first mechanically polished with $0.05 \mu\text{m}$ polishing alumina and then given a final surface treatment using one of two methods:

(1) electropolishing for 5 min with a solution of 250 mL ethanol, 50 mL perchloric acid at 0 °C, 15V DC and a graphite cathode or (2) etching with 1% hydrofluoric acid solution for 2 min at room temperature. Both of the etchants were suitable for EBSD specimen preparation.

2.4 Electron Backscattered Diffraction (EBSD)

Coupons with the various geometries in Fig. 3 were analyzed for crystallographic texture using electron backscattered diffraction (EBSD). Electron backscattered diffraction is a point analysis technique in which the electron beam is focused on a small area of the order of a few microns or smaller. The backscattered electrons from the specimen are diffracted and form Kossel cones, which are intercepted on a phosphor screen. The apex angle of the cones is close to 180°, so the intersections of the cones with the screen are straight lines which form bands called Kikuchi bands. The Kikuchi bands

Table 4 Surface identification for the longitudinal sections in Fig. 3(b)

Slice/Surface Number	Identification
Top/1 and 2	Top surface (1) and surface next to cut (2)
Middle/3 and 4	Both surfaces next to cuts; surface 3 opposite surface 2
Bottom/5 and 6	Surface next to cut (5) and bottom surface (6)

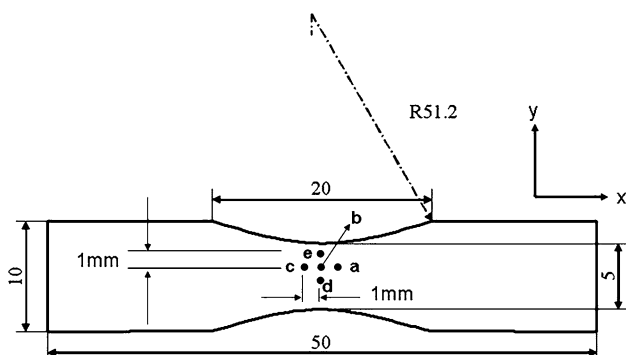


Fig. 4 Schematic showing EBSD locations (marked by black circles labeled with letters “a” through “e”) on longitudinal sections cut from friction stir processed tensile coupons. All dimensions in mm

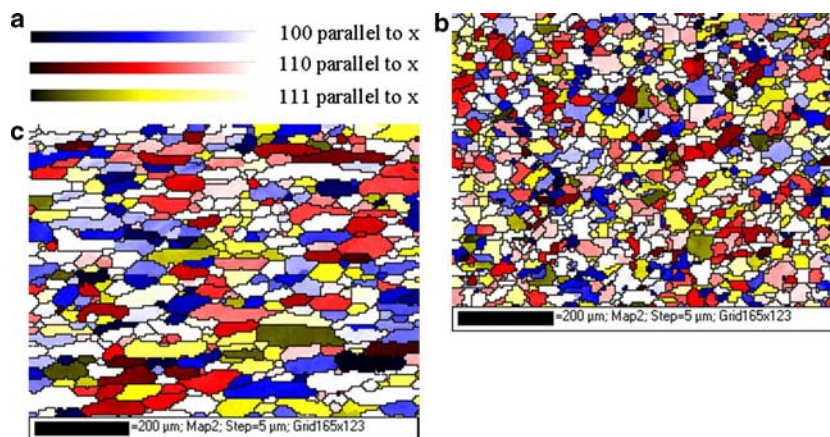


Fig. 5 EBSD maps of (b) AA5182-O, and (c) AA6111-T4 base materials (acquired from transverse sections). EBSD data are rotated to match the coordinate axes shown in Fig. 1. Color code is in (a)

can be indexed to identify the crystallographic orientation at that location in the specimen. This process is repeated at a large number of points to scan a large area and data can be used to create a crystallographic map of the specimen (Ref 7).

EBSD was performed in a JEOL 845 scanning electron microscope using the Channel 5 software from HKL Technology, Inc. (Ref 13). A 60° tilt and step sizes of 0.75-5 μm were used for data collection. Coupons were mounted such that the width section (6.4 mm) was visible. EBSD maps from several areas were stitched together to create a map of a larger region. Subsets from these maps were then selected and used to plot pole figures and inverse pole figures in a local region using the Channel 5 software from HKL Technology, Inc. The texture intensity values were obtained from the pole figures and inverse pole figures.

During EBSD data collection, the sample was arranged so that the *x*-direction was parallel to the tool translation direction, the *y*-direction was in the plane of the sample but perpendicular to the translation direction, and the *z*-direction was normal to the sample surface (i.e., parallel to the tool rotation axis). On each longitudinal surface, the EBSD runs covered an area of about 0.3-0.5 mm in the *x*-direction and 0.2-0.3 mm in the *y*-direction.

On the longitudinal sections (see Fig. 3b), EBSD was performed on surfaces 1, 2, 5, and 6 to obtain a complete texture distribution with depth through the friction stir processed zone (see Table 4). Surfaces 3 and 4 were next to surfaces 2 and 5, respectively, and were thus not expected to provide any additional information. EBSD maps were obtained at five locations on each surface. A schematic of these locations is shown in Fig. 4 in which the EBSD locations are marked with solid circles labeled with letters ‘a’ through ‘e’. Each location was ~1 mm away from an adjacent location. The EBSD runs covered between 0.3 and 0.5 mm in the *x*-direction and 0.2-0.3 mm in the *y*-direction (see Fig. 1). Note that the orientations of surfaces 2 and 6 were rotated by 180° around the *x*-axis relative to surface 1 since surfaces 1 and 2 were the opposite sides of the same coupon and similarly, surfaces 5 and 6 were the opposite sides of the same section. However, all data used in this study were rotated appropriately to match the coordinate system shown in Fig. 1. On the transverse coupons, EBSD maps were obtained at nine locations making a 3 × 3 grid across and covering the entire depth of the friction stir processed region. The orientation of the transverse specimens was kept such that the *x*, *y*, and *z* directions were parallel to *y*, *z*,

and x , respectively, in Fig. 1. EBSD data taken from transverse coupons were also rotated to match the coordinate axes used for longitudinal sections. All EBSD data for friction stir processed material, therefore, have coordinate axes consistent with Fig. 1 and follow the color scheme in Fig. 5.

3. Electron Backscattered Diffraction Analysis

Electron backscattered diffraction maps taken from AA5182-O and AA6111-T4 base material are shown in

Fig. 5, with the color scheme used for all EBSD results given in (a) at the top of the figure. The EBSD maps in Fig. 5 were taken from a region outside of the friction stir processed material from selected transverse sections (see Fig. 3c). The average grain sizes were measured to be 21.3 and 35.3 μm for AA5182-O and AA6111-T4, respectively. Grain size measurement was made with the HKL Channel 5 software by detecting grain boundaries with a misorientation angle greater than or equal to 10° . Figure 5 shows that the base material in both alloys has a random texture.

In the friction stir processed regions, we found variations in texture, grain shape and size with depth in the coupons and also

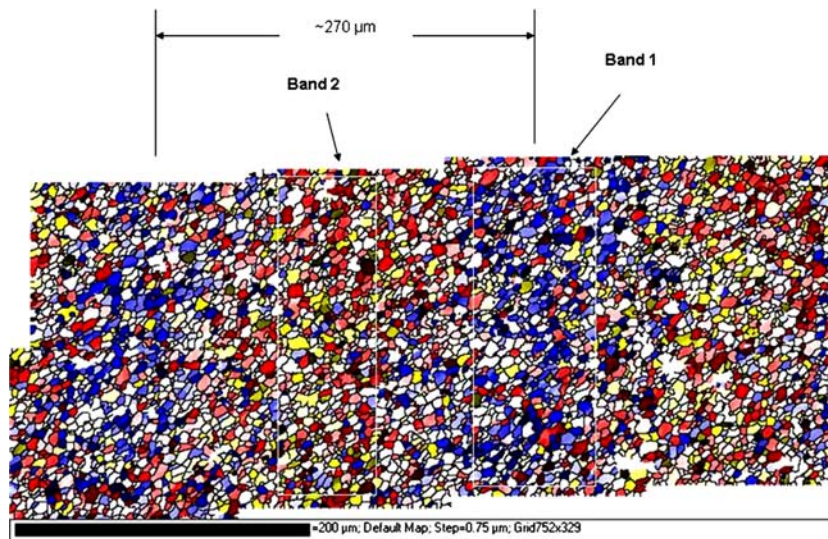


Fig. 6 EBSD map taken from a region of the centerline of the friction stir processed zone on surface 1 of an AA5182-O longitudinal section. The orientations are color-coded as shown in Fig. 5. Two distinct bands of crystallographic texture are observed

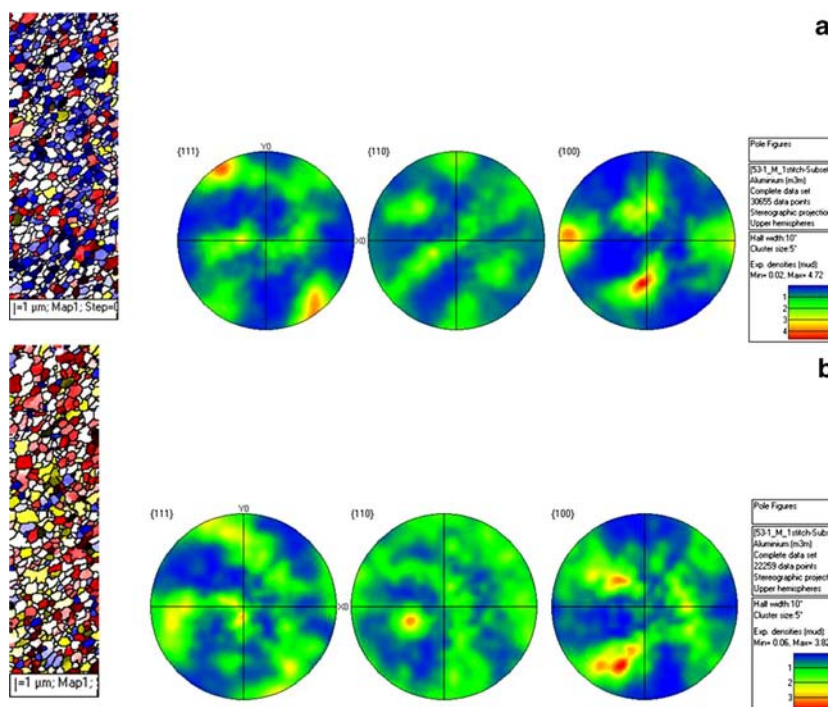


Fig. 7 EBSD subset maps with the corresponding pole figures for bands in Fig. 6. (a) Band 1 EBSD subset map and corresponding pole figures. (b) Band 2 EBSD subset map and corresponding pole figures

on a given coupon surface. These observations are discussed below.

3.1 AA5182-O: Longitudinal Section

An EBSD map taken from location 'a' on surface 1 of an AA5182-O friction stir processed longitudinal section is shown in Fig. 6. The average grain size is $\sim 4.7 \mu\text{m}$. It can easily be seen from Fig. 6 that the grains are oriented in bands of different textures where one band has a majority of blue colored grains (called band 1) while the other does not have a dominant color (called band 2). Subsets from each of these bands were selected and used to plot pole figures. These subsets and their corresponding pole figures are shown in Fig. 7. Note that Y0 points to the advancing side of the friction stir processed region; while X0 corresponds to the direction of tool translation (see Fig. 1). In band 1, the grains are oriented such that the $\langle 001 \rangle$ crystallographic direction is parallel to x , or parallel to the direction of tool translation as can be seen from the blue color in the EBSD map in Fig. 7(a) (far left). The (100) pole figure for band 1, given in Fig. 7(a) (far right) shows that one of the $\{100\}$ poles is oriented parallel to the x -axis and the other two are oriented along a direction between the y and z axes. The intensity of texture is 4.72 times that of the uniform distribution. In addition, a $\langle 111 \rangle$ texture component is also observed. We can see from the (100) pole figure in Fig. 7(b) that in band 2, $\{100\}$ poles are not strongly oriented in any particular direction and this results in the bands in the pole figure. Also, the maximum intensity in Fig. 7(b) is only 3.8 times that of a uniform distribution.

A scanning electron microscope image of surface 1 in Fig. 8(a) shows bands on the coupon surface that are characteristic of friction stir processing. These bands, which vary in width (i.e. by as much as an order of magnitude) and separation, are formed periodically from the rear of the tool. Band separation along the centerline of the friction stir processed zone is typically the same as the distance traversed during one rotation of the tool ($\sim 268 \mu\text{m}$) (Ref 3). The distance between the similarly colored bands in the EBSD map shown in Fig. 6 is $\sim 270 \mu\text{m}$, as indicated, and these are indicative of texture along the centerline. The narrowest separation in Fig. 8(a) is $\sim 207 \mu\text{m}$ which is along the advancing edge of the friction stir processed zone where band separation is smallest. It can also be observed in Fig. 8(a) that the bands are prominent only in the top half of the image while the bands are largely out of focus in the lower half. This is due to the severe inclination of the friction stir weld region.

To further investigate the bands observed in the SEM micrograph, we analyzed the EBSD maps from locations 'd' and 'e' as shown in Fig. 4. An EBSD map taken from location 'e' is shown in Fig. 8(b). The texture bands are not well defined in this figure but the map shows alternate bands of fine and large grains. The separation between two bands of fine grains (marked by arrows) is $\sim 195 \mu\text{m}$. The widths of large grained and fine grained bands are ~ 170 and $25 \mu\text{m}$, respectively. The widths and separation of the bands in Fig. 8(b) agree well with the bands observed in Fig. 8(a), which suggests that the bands of fine grains correspond to the narrow bands observed in the SEM micrograph.

Location 'd' (see Fig. 4) showed texture bands similar to those shown in Fig. 6 but the bands were not well defined. Also, the bands of varying grain sizes were not observed at location 'd'. In summary, it is observed that the bands of

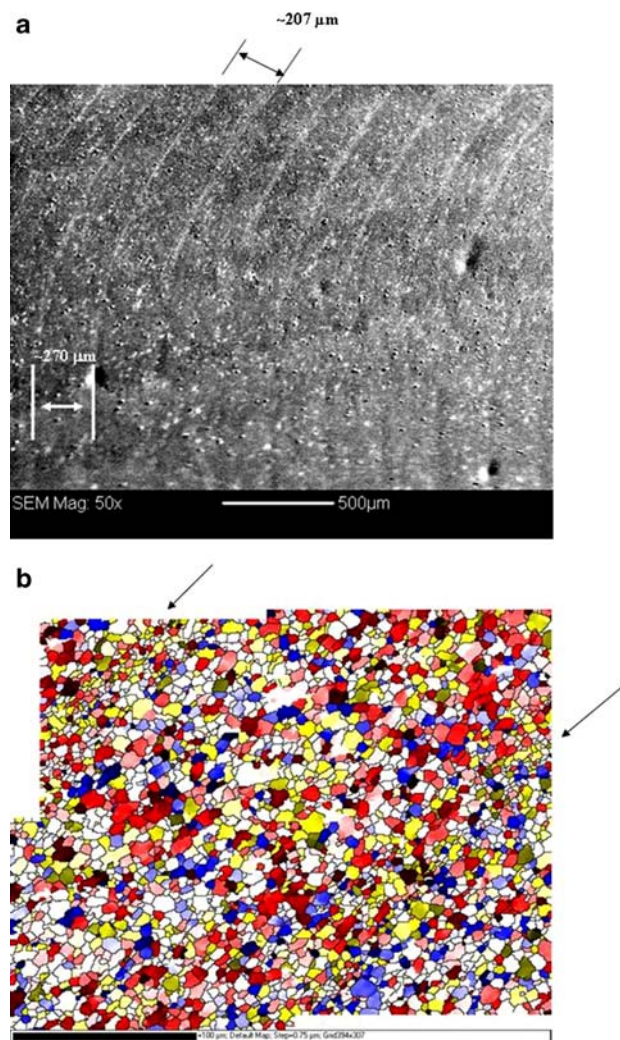


Fig. 8 (a) SEM image of surface 1 of a friction stir processed AA5182-O longitudinal section. The top horizontal line of the image is closest to the advancing edge of the friction stir processed zone. (b) EBSD map on the AA5182-O surface in Fig. 8(a) from location 'e' (advancing edge) as denoted in Fig. 4. Note the bands of fine grains marked by the arrows

varying grain sizes form on the advancing side while the retreating side and the stir processed zone centerline had bands of varying texture, which were not well defined.

As mentioned previously, EBSD maps were obtained at five locations (shown in Fig. 4) on each surface of the longitudinal coupons to study texture variations across a surface. Pole figures were plotted from these maps and subsets selected from band 1 of each of these maps. In Fig. 9, the pole figures for five locations are arranged according to the relative positions on the specimen where each location was separated from the adjacent location by ~ 1 mm. Figure 9(a) shows pole figures from large regions including both bands 1 and 2 and Fig. 9(b) shows pole figures from band 1 only. The maximum texture intensity for each pole figure (where numbers indicate the pole concentration in multiples of uniform distribution) and the average grain size for the corresponding subset are given below each set of pole figures. It can be observed that along the x -direction (or the direction of tool translation), the texture and texture intensity remain nearly unchanged. Moving in the positive y -direction,

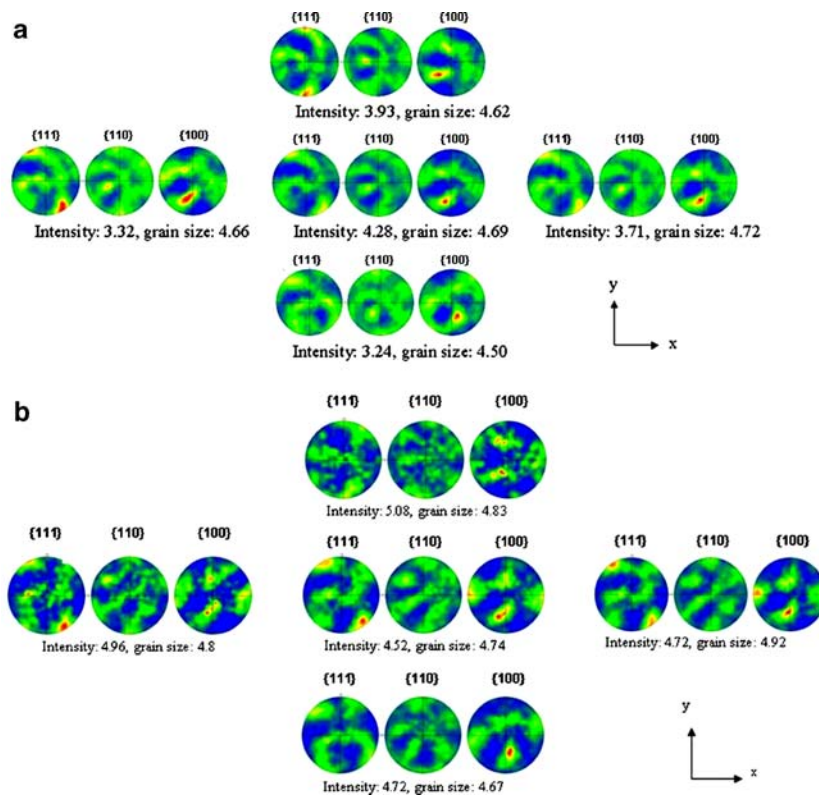


Fig. 9 Pole figures from locations a-e (see Fig. 4) on surface 1 of AA5182-O. Grain sizes are in microns. (a) Pole figures due to averaging of bands 1 and 2. (b) Pole figures constructed from band 1 only

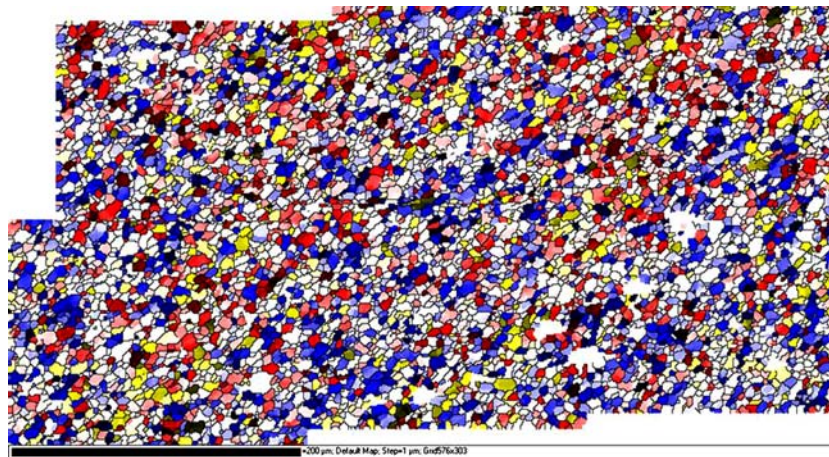


Fig. 10 EBSD map taken from the region of weld centerline on surface 2 (see Fig. 3b) of AA5182-O friction stir processed material. Note diffuse banding of varying textures

the {100} poles are rotated clockwise (in the direction of tool rotation, see Fig. 1) around the z-axis (i.e., normal to the page). This rotation of {100} poles can be clearly seen from the pole figures arranged in the vertical direction in Fig. 9. Additionally, an alignment of {111} poles parallel to y can be observed at location ‘e’ (i.e., on the advancing side). Another point to be observed from Fig. 9(a) is that one of the {100} poles is oriented in a particular direction and the other two {100} poles are randomly oriented which results in the formation of a band in the pole figure.

Rotation of average texture components was observed when moving along the positive y-direction on surfaces 2 and 5, but the bands of varying texture were not well defined. Figure 10 shows an EBSD map taken from surface 2 of an AA5182-O friction stir processed coupon. Note that diffuse banding of alternate “blue-dominated” and “random-colored” regions can be seen. Also, the texture intensity decreased when going deeper into the stir processed zone and surface 5 had a pole density of only 2-3 times that of uniform distribution (an observation to be addressed shortly). Bands of fine grains were

observed on surfaces 2 and 5 also. As was the case with surface 1, these bands were present only on the advancing side of the stir processed zone (at or around location 'e' in Fig. 4). EBSD maps taken from the advancing side on surfaces 2 and 5 are given in Fig. 11. The bands in Fig. 11(b) are tilted in the opposite direction than those in Fig. 11(a) because during EBSD data collection, this coupon was aligned at 180° to the orientation specified previously. However, data were rotated appropriately to match the coordinate axes shown in Fig. 1. The separation between two bands (center to center) of fine grains was found to be ~ 150 and ~ 116 μm on surfaces 2 and 5, respectively. It should be noted that these bands are much closer on surface 5 than on surfaces 1 and 2 and that the separation of the bands decreases with depth into the friction stir processed region (as expected). We can also see from Fig. 11(b) that surface 5 had a much larger region of fine grains compared to surfaces 1 and 2. Surface 6 had only the base material and it was not characterized in detail.

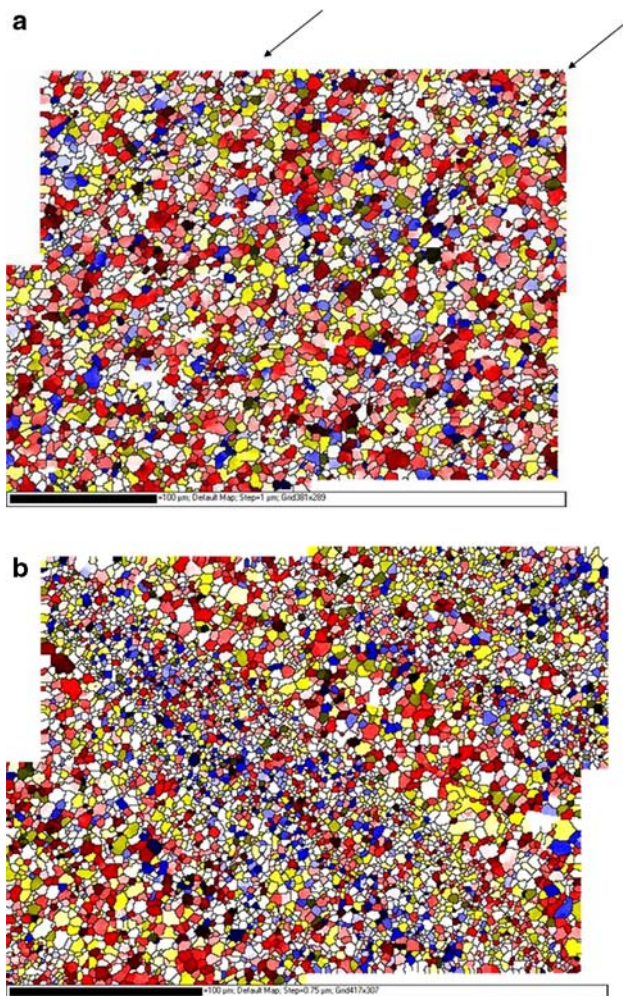


Fig. 11 (a) EBSD maps taken from the advancing edge (location 'e' in Fig. 6) in surface 2. The bands of fine grains are marked by the two arrows at the top of the figure. (b) EBSD maps taken from the advancing edge (location 'e' in Fig. 4) in surface 5 (see Fig. 3b) of AA5182-O friction stir processed material. The bands are tilted in the opposite direction than in Fig. 11(a) because during EBSD data collection, the specimen was aligned at 180° to the convention used throughout the study. However, the crystallographic data are rotated to match the coordinate system orientation in Fig. 1

Within a given surface, the average grain size was constant except on surface 5 where a $1\ \mu\text{m}$ change in grain size was observed along the y -direction. The texture intensity was found to decrease with depth into the friction stir processed zone (i.e., in moving from the surface that was in contact with the tool into the material). Also, the grain size varied as a function of depth inside the section.

3.2 AA6111-T4: Longitudinal Section

An EBSD map taken from surface 1 of longitudinal sections of AA6111-T4 friction stir processed material is shown in Fig. 12 in which the average grain size is $\sim 4.2\ \mu\text{m}$. The grains are oriented in bands of different textures as on surface 1 of the AA5182-O friction stir processed material. These bands are labeled I and II to differentiate from bands 1 and 2 in AA5182-O. The band with blue as a dominant color will be called band I. Figure 13 shows the subsets selected from the EBSD map in Fig. 12 and their corresponding pole figures. Though the blue color in Fig. 12 means an alignment of $\langle 001 \rangle$ parallel to x -axis, it can be seen from the pole figures in Fig. 13 that in both bands I and II, one of the $\{100\}$ poles was aligned parallel to the z -axis and the two other poles were oriented in specific directions close to the x and y axes. This orientation leads to the colors observed in Fig. 12. The orientations in bands I and II are very similar with only a slight rotation of $\{100\}$ poles from band I to band II. The strong alignment of all three $\{100\}$ poles in specific directions leads to strong texture intensity and also to pole concentration in the $\{111\}$ and $\{110\}$ pole figures. The texture intensity in Fig. 13 is ~ 8 and 14 times the uniform distribution in bands I and II, respectively.

Figure 14 shows the pole figures plotted for bands I and II taken from the EBSD maps obtained from five locations on surface 1 as shown in Fig. 4. The pole figures are arranged according to the relative position of the EBSD location on the coupon surface. The maximum texture intensities and average grain sizes for the corresponding EBSD subsets are given below each pole figure. The observations from this figure are similar to those made for AA5182-O friction stir processed material in Fig. 9 although the texture is stronger in the AA6111-T4 friction stir processed material. We can see that in both bands I and II, the $\{100\}$ poles are rotated in the direction of tool rotation when moving along the $+y$ -direction and the pole orientations remain unchanged in the x -direction, which is same as the direction of tool advancement. In general, the texture intensity did not vary significantly in Fig. 14 except in the y -direction for band I where the intensity increases from 6 to 15.

Other longitudinal surfaces investigated for this alloy (2, 5, and 6 in Fig. 3b) also showed a rotation of texture components around the z -axis when moving along the $+y$ -direction. However, the texture rotations were difficult to identify on surface 6 because of a relatively weak texture (4-6 times the uniform distribution) compared to surface 1 (8-15 times uniform distribution). Texture bands, which were observed on surface 1, were not well defined on all other surfaces. Surface 5 exhibited equiaxed grains with random texture (Ref 5, 8). Representative EBSD maps from surfaces 2 and 5 are shown in Fig. 15. Unlike the AA5182-O friction stir processed material, no well-defined bands of fine grains were observed on any of the surfaces but several small clusters of fine grains were observed especially on surfaces 5 and 6. Such clusters can be seen in Fig. 15(b).

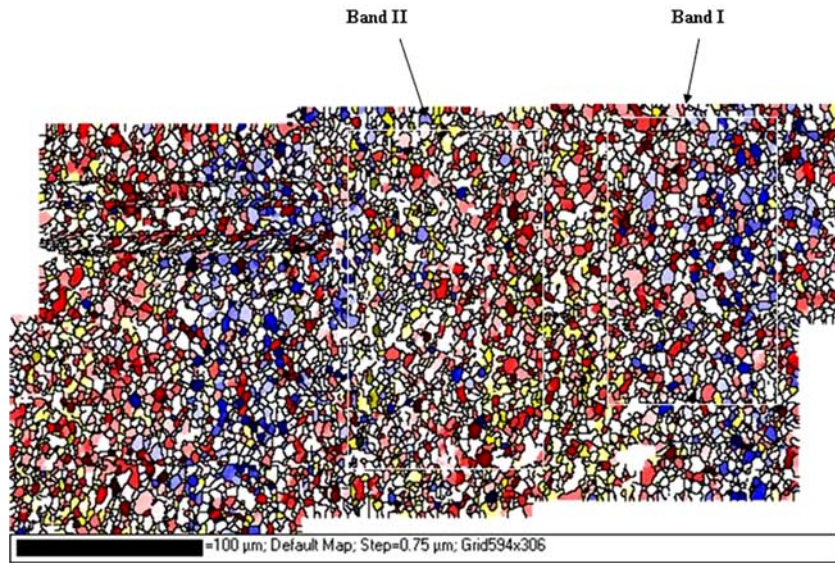


Fig. 12 EBSD map taken from a region close to the centerline on surface 1 (see Fig. 3b) of AA6111-T4 friction stir processed material

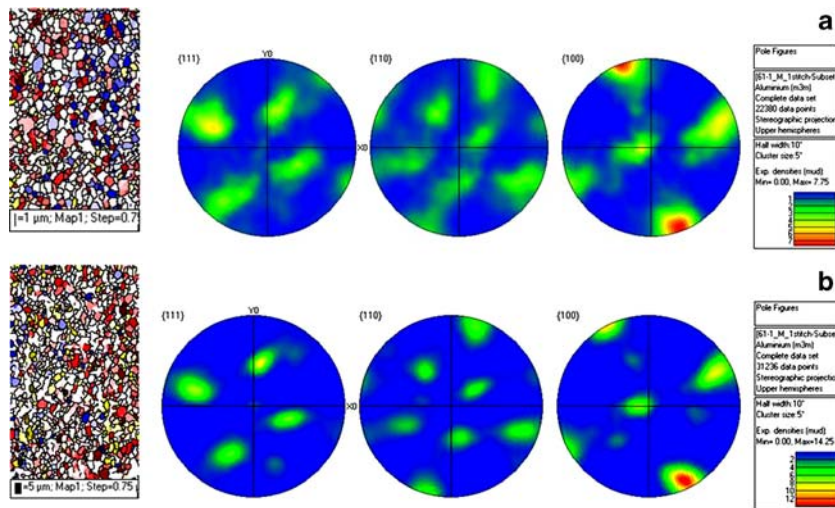


Fig. 13 EBSD subset maps for AA6111-T4 with the corresponding pole figures for bands (from Fig. 12). (a) Band I (with blue color dominance) EBSD subset map and corresponding pole figures. (b) Band II EBSD subset map and corresponding pole figures

Within a given surface, the average grain size was constant except on surface 5 where a 1 μm change in grain size was observed along the y -direction. Note that this change is significant in comparison to the average grain size which ranged between 4 and 6 μm . This observation is the same as that made for the AA5182-O friction stir processed material. Changes in average grain size on all other surfaces were less than 0.5 μm . The grain size was also largest on surface 5. A histogram of AA6111-T4 grain sizes on different surfaces is also given in Fig. 16. Both materials showed a similar variation in grain size with depth though the change in grain size was larger in AA6111-T4 material than in the AA5182-O material.

All materials in the friction stir processed region are dynamically recrystallized because the grain size in this region (4–7 μm) is much smaller than the starting grain size (20–30 μm) in both alloys. It is interesting to note that in the friction stir processed zones of both AA5182-O and AA6111-T4,

{100} poles were oriented in specific directions and that these poles were rotated in the direction of the tool rotation. This implies that the friction stir processed regions have a recrystallization texture in which {100} poles are preferably oriented in some directions which, in turn can be rotated in the direction of the tool rotation due to repeated mechanical work. It should be noted that the time for which any region experiences severe mechanical deformation is the time it takes for the tool to advance by a distance equal to its diameter. The rotation of {100} poles that is observed in this study is probably caused during a single rotation of the tool as the tool advances and leaves plastically worked material in its wake.

3.3 Transverse Sections

Analysis of the transverse sections (see Fig. 3(c) for coupon geometry) revealed that the interface between the friction stir processed zone and the thermomechanically affected zone

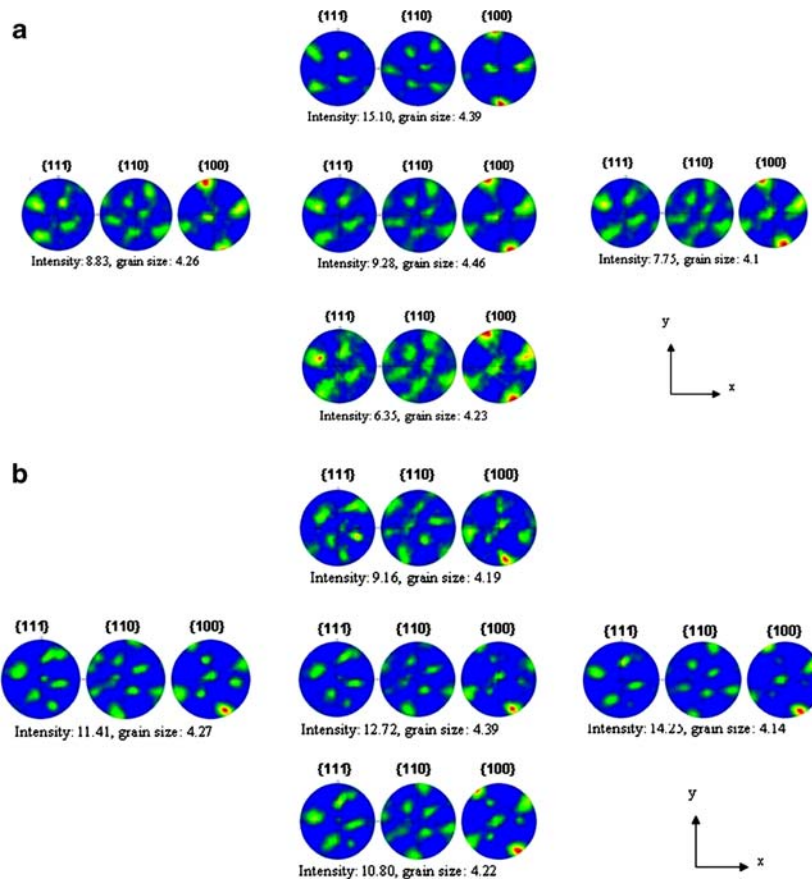


Fig. 14 Pole figures from locations a-e (see Fig. 6) on surface 1 (see Fig. 3b) of friction stir processed AA6111-T4 material. (a) Pole figures constructed from band I only. (b) Pole figures constructed from band II only

(TMAZ) has a small slope close to the top surface. This can be seen from Fig. 17(a), which shows an EBSD map from the advancing edge close to top surface in an AA5182-O friction stir processed material. Figure 17(b) shows the advancing edge deeper inside the friction stir processed region of AA6111-T4. The interface between the friction stir processed zone and the TMAZ is steeper in Fig. 17(b) than in Fig. 17(a).

Observations related to crystallographic texture made from longitudinal sections were further confirmed by analyzing transverse sections. EBSD maps taken from regions close to the top edge of transverse sections showed a texture orientation the same as that seen on surface 1 of longitudinal sections from both AA5182-O and AA6111-T4 friction stir processed materials. In addition, moving from the advancing edge to the retreating edge, the same rotation of texture components (around the z-axis) was observed as on the longitudinal sections. It was found that the texture close to the top edge was significantly different than the material immediately below the top surface. This can be seen in Fig. 18, which shows an EBSD map taken from a region along the friction stir processed material centerline, close to the top edge on the transverse section of the AA5182-O material. The top layer of similarly oriented grains was less than 100 μm thick and the thickness of this top layer decreased in regions close to the stir processed/TMAZ interface. This was observed for both alloys. An analysis of pole figures showed that in the AA5182-O friction stir processed material, the texture was random immediately below the top surface while a gradual decrease in texture intensity was observed in the AA6111-T4 friction stir processed material.

Analysis of transverse sections also enabled us to study texture and grain size as a function of depth. Figure 19 shows pole figures obtained from EBSD maps taken along the friction stir processed zone centerline at different depths in both the materials. The maximum texture intensity for each pole figure and the grain size in the corresponding EBSD maps are given below each pole figure. The grain sizes are those on the transverse sections. It can be seen that the texture becomes weaker moving further into the friction stir processed zone. The pole orientation also appears to change as a function of depth but it should be noted that the intensity of texture is low in regions close to the bottom of the zone and the red color in the pole figures only shows a relative pole concentration. Also evident from Fig. 19 is the fact that deeper into the zone, the grain size first increases and then decreases. This is consistent with the grain size observations from the longitudinal sections as shown in Fig. 16. Figure 20 shows a plot of grain size as a function of depth into the friction stir processed materials. For both materials, the grain size increases to a maximum value and then decreases deeper into the friction stir processed zone. A difference in grain size is also observed between the advancing side, friction stir processed zone centerline and the retreating side. The average grain size as well as the change in grain size is greater in AA6111-T4 material than in AA5182-O material. We can also see from Fig. 20 that the advancing side tends to have a smaller grain size compared to the retreating side in both materials.

The transverse sections also revealed differences between the morphology of the advancing and retreating sides of the

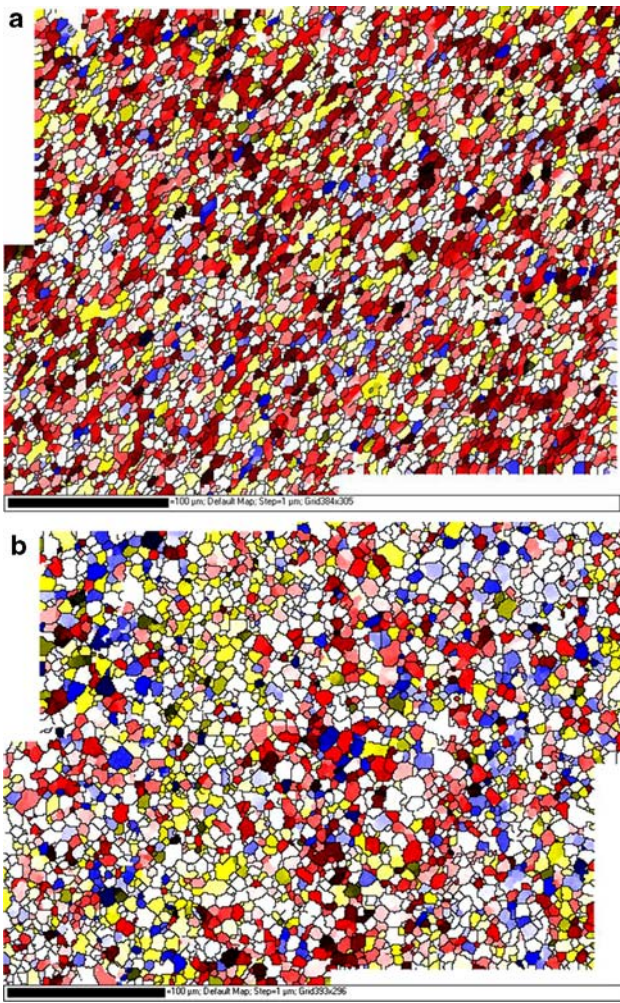


Fig. 15 EBSD maps taken from the centerline region of friction stir processed AA6111-T4 material. (a) Surface 2. (b) Surface 5. Note clusters of fine grains

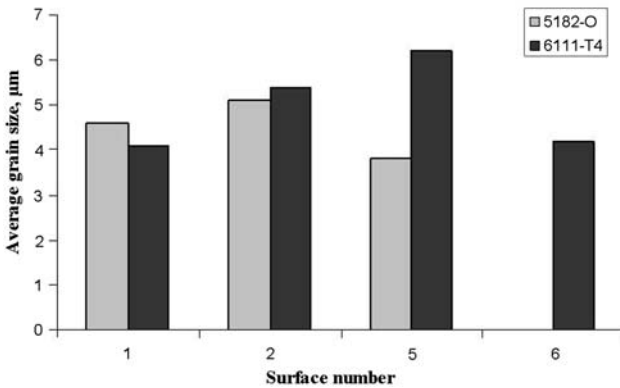


Fig. 16 Histogram showing average grain sizes on the various longitudinal surfaces investigated for AA5182-O and AA6111-T4 friction stir processed material

friction stir processed zone. The advancing side had a relatively well-defined interface between the stir processed zone and TMAZ, whereas the interface on the retreating side had a complex microstructure with a mixed distribution of large and

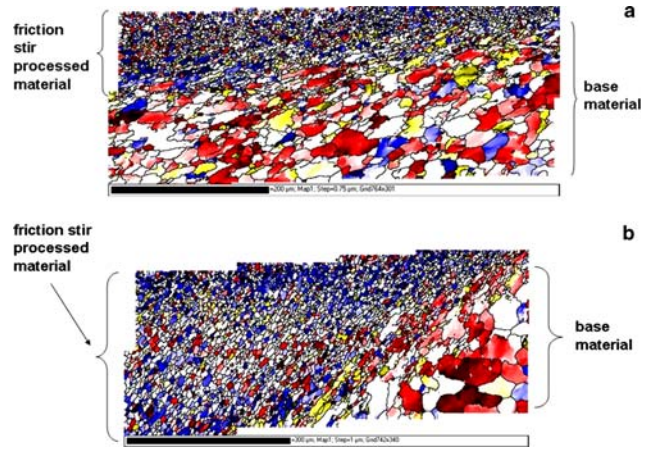


Fig. 17 (a) EBSD maps obtained on the transverse coupons (see Fig. 3c) from the tool advancing edge (see Fig. 1), close to the top surface in AA5182-O. (b) EBSD maps obtained on a transverse coupon (see Fig. 3c) from the tool advancing edge (see Fig. 1), deeper inside AA6111-T4

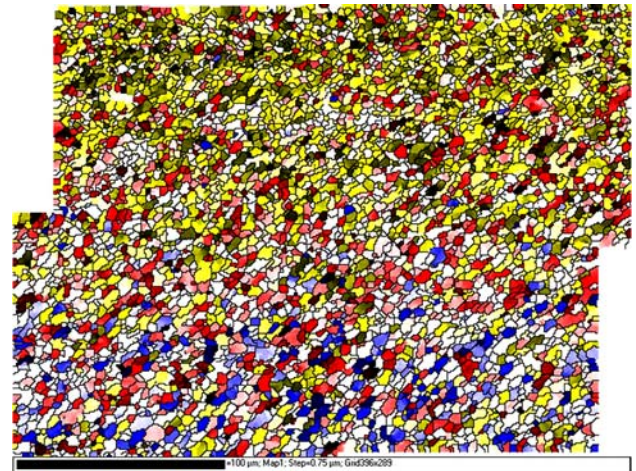


Fig. 18 EBSD map taken from a region along the weld centerline, close to the top surface of a transverse coupon (see Fig. 3c) of AA5182-O. The map shows different grain orientations at the top and immediately below top surface

small grains. Figure 21(a) and (b) show EBSD maps from the retreating sides of the AA5182-O and AA6111-T4 friction stir processed zones, respectively. In comparison with Fig. 17, we note that the interface between the friction stir processed zone and the TMAZ on the advancing side is well-defined relative to that on the retreating side. This observation has also been reported by HKL Inc. (Ref 8).

4. Concluding Remarks

Both AA5182-O and AA6111-T4 friction stir processed materials contain a crystallographic texture, in which {100} poles are oriented in certain directions. In AA5182-O, one of the {100} poles is aligned parallel to the *x*-axis or tool translation axis, while the other two poles are randomly oriented. In AA6111-T4 friction stir processed material, all

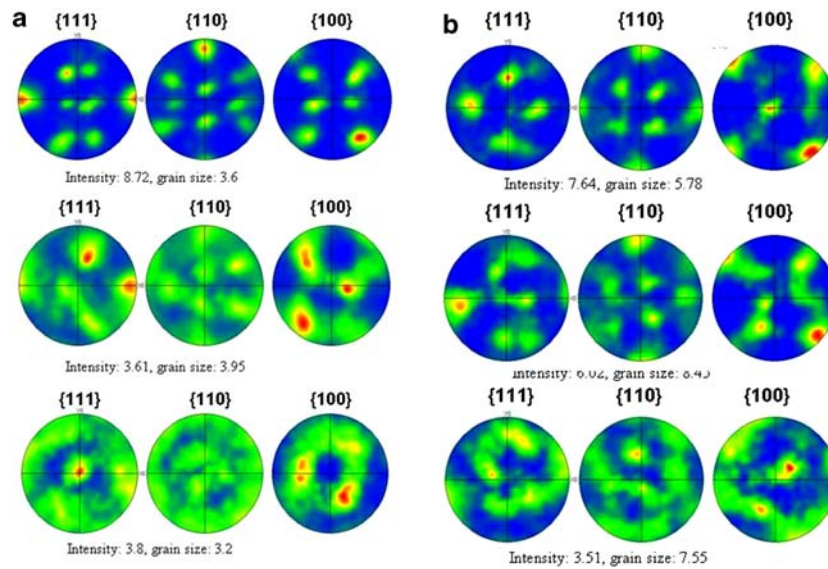


Fig. 19 Pole figures constructed from EBSD maps taken along the weld centerline at different depths. The depth increases from top to bottom. Note that the texture intensity decreases deeper into the friction stir processed material. Grain size is in microns. (a) AA5182-O. (b) AA6111-T4

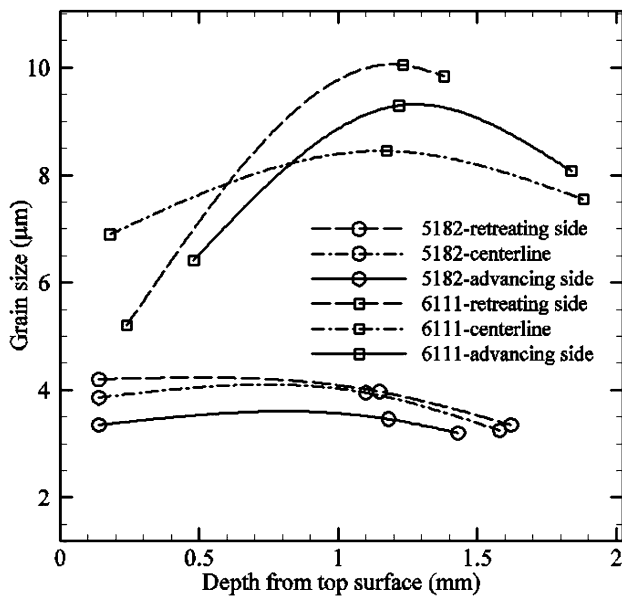


Fig. 20 Plot showing transverse grain size as a function of depth from top surface (see Fig. 3b) for advancing edge, retreating edge (see Fig. 1) and the centerline in friction stir processed AA5182-O and AA6111-T4

three {100} poles are aligned in specific directions, one of which was the z -axis. This texture is primarily localized on the top surface of the coupons examined (i.e., the surface that came into contact with the tool) and the texture becomes weaker with increasing depth into the friction stir processed zone (i.e., perpendicular to the top surface). The loss of texture with depth is more gradual in the AA6111-T4 material than in the AA5182-O material. The top surfaces in both materials also display banding of crystallographic texture such that the poles are slightly rotated between the two bands. Within a given surface, the texture as well as grain size essentially remains unchanged in the direction of the tool advancement, while the

{100} poles in both materials are rotated in the direction of tool rotation as when moving along the in-plane direction perpendicular to the tool advancement direction. The overall texture is stronger in the AA6111-T4 material than in the AA5182-O material. This appears to be a material effect because similar observations were made when comparing laser welds in these two materials (Ref 11). Therefore, AA6111-T4 is more susceptible to developing crystallographic texture than AA5182-O during friction stir processing.

The AA5182-O friction stir processed material shows bands of small grains which are very prominent on the advancing side of the tool. The spacing between these bands is typically the same as the distance advanced by the tool in one rotation. These bands can also be seen in SEM images taken from the top surface (surface 1) of the AA5182-O material. The spacing between the bands of small grains is observed to decrease at greater depths into the friction stir processed zone. Such bands of small grains are not found on the top surface of the AA6111-T4 material, although several clusters of small grains are found on surfaces 5 and 6. Also, from Fig. 16 and 20, it is clear that the two materials have similar grain sizes in regions close to the tool. However, in regions remote from the top surface, the AA6111-T4 material has a larger grain size than the AA5182-O material. Also the grain size is seen to increase and then decrease with increasing depth into the friction stir processed zones suggesting a variable grain size distribution.

Both alloys show significant differences between the advancing and retreating sides of the friction stir processed zone. Differences are observed in grain size, texture, and the interface between the friction stir processed zone and the TMAZ. The advancing side has a smaller grain size than the retreating side. In general, texture is stronger on the advancing side than on the retreating side and poles are rotated in the direction of tool rotation when going from one side to the other. The interface between the friction stir processed zone and the TMAZ is relatively sharp on the advancing side, while a complex microstructure composed of both large and small grains is observed on the retreating side.

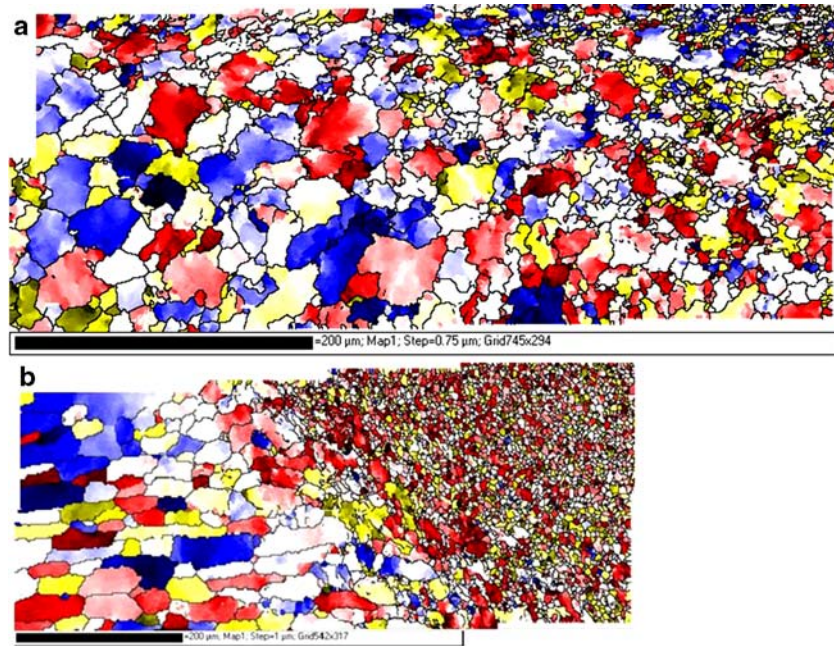


Fig. 21 EBSD maps taken from the retreating edges of both alloys. A complex microstructure with large and small grains can be observed at the interface between the main portion of the friction stir processed zone and the thermomechanically affected zone (TMAZ). (a) EBSD map of retreating edge in AA5182-O. (b) EBSD map of retreating edge in AA6111-T4

There are some interesting texture differences between laser and friction stir processed AA5182-O and AA6111-T4. For example, only columnar grains on the edges (i.e., boundary between the fusion and HAZ zones) of the Nd:YAG laser processed materials are textured (Ref 11). However, in the friction stir processed materials investigated in the present work, it is the equiaxed grains that are textured. Columnar grains form in laser welding due to solidification, while equiaxed grains predominate in friction stir processing (and in friction stir welded materials as well) due to recrystallization. In laser welded AA5182-O, the $\langle 001 \rangle$ poles are aligned parallel to the axis of columnar grains. In friction stir processed AA5182-O, the $\langle 001 \rangle$ poles are aligned parallel to the direction of tool advancement.

In the second part, tensile mechanical properties of friction stir processed AA5182-O and AA6111-T4 are quantified using a state-of-the-art digital image correlation technique. The impact of crystallographic texture (determined in Part 1) on tensile properties is explored in this latter part in order to tie up the work in both parts.

References

1. W.M. Thomas, E.D. Nicholas, J.C. Needham, M.G. Murch, P. Temple-Smith, and C.J. Dawes, "Friction Stir Butt Welding," GB Patent No. 9125978.8, International Patent No. PCT/GB92/02203, 1991
2. K. Colligan, Material Flow Behavior During Friction Stir Welding of Aluminum, *Welding Research Supplement*, *Welding J.*, 1999, **78**, p 229.s–237.s
3. J.A. Schneider and A.C. Nunes Jr, Characterization of Plastic Flow and Resulting Microtextures in a Friction Stir Weld, *Metall. Mater. Trans. B*, 2004, **35**, p 777–783
4. T.U. Seidel and A.P. Reynolds, Visualization of the Material Flow in AA2195 Friction Stir Welds using a Marker Insert Technique, *Metall. Mater. Trans. A*, 2001, **32**, p 2879–2884
5. D.P. Field, T.W. Nelson, Y. Hovanski, and K.V. Jata, Heterogeneity of Crystallographic Texture in Friction Stir welds of Aluminum, *Metall. Mater. Trans. A*, 2001, **32**, p 2869–2877
6. [<http://www.aluminum.org/ANTemplate.cfm?IssueDate=11/01/2005&Template=/ContentManagement/ContentDisplay.cfm&ContentID=9294>]
7. A.J. Schwartz, M. Kumar, and B.L. Adams, *Electron Backscatter Diffraction in Materials Science*. Kluwer academic/Plenum publishers, New York (NY), 2000
8. Characterizing texture variations in a friction stir welded aluminum alloy. <http://www.hkltechnology.com/data/0-FSW-aluminium.pdf>
9. Y.S. Sato, H. Hiroyuki, K. Ikeda, M. Enomoto, S. Jogan, and T. Hashimoto, Microtexture in the Friction-Stir Weld of an Aluminum Alloy, *Metall. Mater. Trans. A*, 2001, **32**, p 941–948
10. H. Jin, S. Saimoto, M. Ball, and P.L. Threadgill, Characterization of Microstructure and Texture in Friction Stir Welded Joints of 5754 and 5182 Aluminum Alloy Sheets, *Mater. Sci. Technol.*, 2001, **17**, p 1605–1614
11. L.G. Hector Jr., Y.-L. Chen, S. Agarwal, and C.L. Briant, Texture Characterization of Autogenous Nd: YAG Laser Welds in AA5182-O and AA6111-T4 Aluminum Alloys, *Metall. Mater. Trans. A.*, 2004, **35**, p 3032–3037
12. L.G. Hector, Jr., Y.-L. Chen, S. Agarwal, and C.L. Briant, "Friction Stir Processed AA5182-O and AA6111-T4 Aluminum Alloys. Part 2: Tensile Properties and Strain Field Evolution," *J. Mater. Eng. Perf.*, in review, 2007, DOI 10.1007/s11665-007-9060-0
13. <http://www.hkltechnology.com/>